Fracture dynamics of correlated percolation on ionomer networks

Yule Wang [1] and Michael Eikerling [2,3,*]

[1]*Department of Physics, Simon Fraser University, Burnaby, British Columbia, Canada V5A 1S6*

[2]*Department of Chemistry and Department of Physics, Simon Fraser University, Burnaby, British Columbia, Canada V5A 1S6*

[3]*Institute of Energy and Climate Research, IEK-13: Modelling and Simulation of Materials in Energy Technology, Forschungszentrum Jülich GmbH, 52425 Jülich, Germany*

(Received 10 October 2019; accepted 25 February 2020; published 7 April 2020; corrected 21 April 2020)

This article presents a random network model to the study fracture dynamics on a scaffold of charged and elastic ionomer bundles that constitute the stable skeleton of a polymer electrolyte membrane. The swelling pressure upon water uptake by this system creates the internal stress under which ionomer bundles undergo breakage. Depending on the local stress and the strength of bundle-to-bundle correlations, different fracture regimes can be observed. We use kinetic Monte Carlo simulations to study these dynamics. The breakage of individual bundles is described with an exponential breakdown rule and the stress transfer from failed to intact bundles is assumed to exhibit a power-law-type spatial decay. A central property considered in the analysis is the frequency distribution of percolation thresholds, which is employed to analyze fracture regimes as a function of the stress and the effective range of stress transfer. Based on this distribution, we introduce an order parameter for the transition from random breakage to crack growth regimes. Moreover, as a practically important outcome, the time to fracture is analyzed as a descriptor for the lifetime of polymer electrolyte membranes.

DOI: 10.1103/PhysRevE.101.042603

I. INTRODUCTION

Fracture formation on structural materials and complex networks is a vital subsubdiscipline of statistical physics [1]. An important goal in this realm is to make a lifetime prediction, i.e., to determine after what time a fracture will form in the system that will lead to the loss of its required function. The historical origin of the field is in the area of textile engineering, where Pierce conducted pioneering theoretical research to study fatigue failure in textile fibers [2]. Other examples of fatigue problems include traffic networks, computer networks, and electrical power grids, as reviewed in Ref. [3].

In electrochemical devices, which are crucial enablers of the global energy transition, the formation and propagation of fractures determines the lifetime of composite porous electrodes and polymer-based electrolytes. These functional components must strike delicate balances as mechanically and chemically robust separators, transport media for gases, solvent molecules, or ionic species, and electrocatalytically active media with a high internal surface area [4].

Polymer electrolyte membranes (PEMs) are key components in fuel cell and electrolyzer devices for low-temperature operation [5]. PEMs are needed in polymer electrolyte fuel cells (PEFCs) as highly transport-selective proton conductors and stable separators between gas compartments on anode and cathode sides. The described functions are crucial to maintain an electrical potential difference that drives reactions in the two electrodes and thus determines the power performance of a cell. The nucleation of cracks and their growth into sample-spanning fractures is a lifetime-limiting event in these systems. If a sample-spanning fracture forms in an operating fuel cell, it will allow high crossover fluxes of reactant gases, viz., hydrogen gas from the anode and oxygen gas from the cathode. This event will cause the breakdown of the fuel cell voltage [6–8].

Past activities in theoretical PEM science have employed molecular dynamics simulations and mean-field theory [9,10] to study the self-assembly of ionomer strands in solution, as illustrated in the upper rail of Fig. 1. These studies have identified cylindrical bundles of ionomer backbones as the prevailing structural motif in the membrane skeleton [11,12]. Stable bundles are assemblies of about 6–20 hydrophobic backbones, resulting in bundle diameters of 3–5 nm. Geometrical bundle parameters could be validated with scattering and microscopy studies [13,14]. Effective cross-linking among bundles occurs because single backbone strands exceed the length of a bundle and therefore participate in neighboring bundles, leading to the emergence of a bundle network. Bundles could assemble further into nanoporous superstructures. Based on this understanding of structure formation in PEMs, a theory of water sorption and swelling was developed, which treats the membrane as a poroelastic medium with highly charged walls [15,16]. The theory of bundle formation provides sizes as well as the density of anionic surface groups and elastic properties of ionomer bundles. The theory of water sorption and swelling gives a statistical distribution of pore sizes and the internal swelling stress (or pressure) in pores, as a function of ionomer molecular structure and external conditions [T and relative humidity (RH)]. The merging point of both theories is a theory of fracture formation in poroelastic PEMs.

Specific challenges in problems of fracture formation in PEMs stem from the presence of a strongly fluctuating

*m.eikerling@fz-juelich.de

 ©2020 American Physical Society

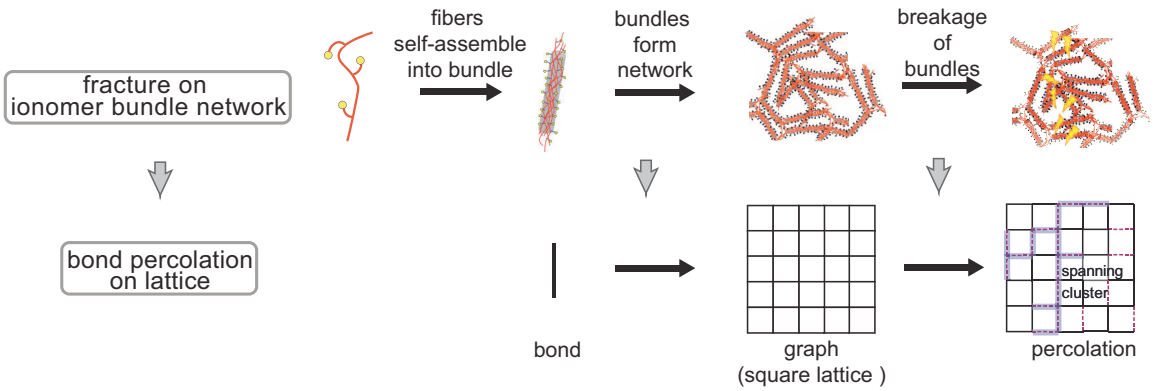

FIG. 1. Ionomer fibers with hydrophobic backbone (red) and grafted side chains (red) terminated with sulfonic acid head groups (yellow) that dissociate in water. The upper rail illustrates self-aggregation into bundles of size k (number of fibers in the bundle) and cross-linking of bundles into a network. In the swollen membrane state, bundles experience an internal of bundles swelling stress that triggers random breakage events. The lower rail illustrates how fracture formation in the bundle network is mapped onto a dynamic bond percolation problem.

internal stress field caused by water sorption. Water uptake and swelling are controlled by the internal osmotic pressure that is balanced by the elastic pressure generated by the bundle network. The random statistical character of the stress field can be gleaned from Fig. 7(b) of Ref. [16]. The network of bundles has to withstand pressures in the order of 10^7 Pa. Elastic properties of ionomer bundles and the local stress they experience are thus as well subject to random distributions. Furthermore, a varying external load could be superimposed, which is caused by the clamping pressures transmitted via flow fields with their characteristic alternating rib and channel structure [17]. The main objective of fracture modeling is to predict the formation time of the first sample-spanning fracture, which represents a primary descriptor of the membrane lifetime.

How does fatigue failure nucleate and how does it propagate in PEMs? Fracture formation is a dynamic network process [1,18–20]. It can be described as a sequence of bundle breakage events that are statistically uncorrelated or correlated. The former case corresponds to the random percolation limit and it was studied by Melchy and Eikerling [21]. In the correlated case, fracture formation is caused by cascading breakages of network elements, which are exponentially accelerated by stress accumulation on surviving bundles. This leads to the follow-up question: How is the mechanical stress or load of a failed bundle redistributed within the remaining intact parts of the network? The answer depends on network properties, stress regime, and the stress-transfer law considered. Here, we study and compare two regimes of load sharing: global load sharing (GLS) [22,23] and local load sharing (LLS) [24].

The theory of fracture formation in PEMs is developed in several steps. The rate of individual bundle breakage will be adopted from previous work, wherein a mathematical rate law as a function of bundle size and local stress was developed [21]. Thereafter, also following Ref. [21], the problem of fracture formation will be mapped onto a graph model. These steps will be revisited in Sec. II. The model developed in Ref. [21] was used to study fracture formation in the regime of weak internal swelling stress, referred to as the random breakage regime. In that work from 2015, an analytical solution was found, which related the time to fracture to network connectivity and dimension, the intrinsic rate of breaking of ionomer fibers and their bundles, the activation volume, and the stress field, assumed as uniform and constant.

When the local stress is more severe, strong spatial correlations and inhomogeneous stress fields invalidate the random percolation approach; this is the case considered in the present work. Local redistribution of stress upon bundle breakage (load sharing) and damage accumulation on surviving bundles favors fracture formation via nucleation and the growth of cracks [1,18,19,25]. For this case, we adopt a kinetic Monte Carlo approach to simulate these processes [26–30]. The specific stress redistribution law dictates the percolation behavior of cracks and the dynamics of fracture formation in different regimes of local stress and correlation among bundles, which can be related to different swelling regimes in PEMs.

II. THE MODEL

The structural membrane motif underlying the development of the percolation model is illustrated in Fig. 1. As we have learned from calculations based on mean-field theory [31–36] and molecular dynamics (MD) simulations [34,37,38], individual ionomer backbone strands in solution assemble into cylindrical bundles. The stable bundle size, given by the number k of strands in a bundle [9,39], results from competing effects of backbone hydrophobicity, favoring phase separation, and electrostatic repulsion due to charged ionic end groups at grafted ionomer side chains, favoring dispersion of ionomer chains in solution. Effective cross-linking of ionomer bundles occurs since the length of a single ionomer strand exceeds the length of a bundle [39]. Upon increasing the ionomer concentration in solution, superstructures of bundles evolve which give rise to the formation of porous membrane morphologies, as seen in numerous scattering studies [12,40,41]. We map this bundle-network morphology onto a random network (graph) model, as illustrated in Fig. 1. The problem of fracture formation thereby becomes a percolation problem. In Fig. 1, each bond represents a cylindrical ionomer bundle formed by k fibers [9,10,21]. The size of a bundle determines its mechanical properties, that is,

its Young's modulus and tensile strength, and its electrostatic properties, viz., the density of charged anionic groups on the bundle surface. These bundle properties determine the water sorption behavior of the membrane, as studied by Eikerling and Berg [15] and Safiollah *et al.* [16], and its propensity to fracture formation [21]. The swelling pressure corresponding to equilibrium water sorption creates the internal stress that triggers bundle breakage events.

In a further simplifying transformation, the random bundle network is replaced by an ordered lattice like structure. In the present work, in order to keep computational costs reasonable, we have considered a bundle network with a two-dimensional square lattice structure, as we were primarily interested in obtaining a qualitative understanding of the impact of correlation effects on fracture formation in this bundle network. In future work, we will consider more realistic and more complex three-dimensional (3D) lattice geometries. The regular lattice of bundles is prepared in an initial state, in which all bundles have equal k and thus equal mechanical strength. Moreover, a uniform initial stress field is assumed, meaning that each bundle in the pristine lattice is intact and under identical stress. In future work, we will relax these assumptions to explore the impact of nonuniformity in bundle properties and the initial stress field.

Fracture formation in the bundle-network model is the consequence of individual bundle breakage events that occur randomly in space and time. Over time, clusters of broken bundles, representing microscopic cracks, grow and increase in density. The stress field evolves and becomes nonuniform. At a certain time, a percolating cluster of broken bundles will emerge, corresponding to a sample-spanning fracture [1,42,43]. In the case of a PEM, this time to fracture, denoted t_{PEM} subsequently, represents the membrane lifetime, as it marks the point at which the membrane becomes transmissive for reactant gases and thereby loses its function as a separator of anode and cathode gas compartments [44].

Individual bundle breakage events could occur in an uncorrelated sequence. This situation corresponds to the random breakage scenario that was studied in Ref. [21]; it is relevant in a regime of low water uptake by the PEM and thus weak swelling stress exerted on pore walls and bundles. However, bundle breakage events could also happen in a highly correlated manner, which is expected in the strong stress regime encountered at large swelling. The latter, more general scenario is the focus of the present work.

Following Ref. [45], the rate of thermally activated breakage of a single ionomer fiber is

$$\kappa_{\mathrm{f}}(\sigma_{\mathrm{f}}) = \tau_0^{-1} \exp\left(-\beta(E_{\mathrm{a}} - \nu\sigma_{\mathrm{f}})\right), \tag{1}$$

where τ_0 is the period of an atomic bond vibration; $\beta = k_{\mathrm{B}}T$, with Boltzmann constant k_{B}; E_{a} the activation energy of fiber breaking; ν the activation volume of an ionomer fiber; and σ_{f} the stress on a single fiber.

Using the assumption of equal load sharing over backbone fibers a bundle, an expression for the breakage rate of a bundle was deduced in Ref. [21], which is given by

$$\kappa_{\mathrm{b}}(\sigma_{\mathrm{f}})^{-1} = \tau_0 \exp(\beta E_{\mathrm{a}}) \sum_{j=1}^{k} \frac{\exp\left(\frac{-k\beta\nu\sigma_{\mathrm{f}}}{j}\right)}{j}. \tag{2}$$

TABLE I. Effective coefficients α_k/α_1 and η_k/η_1 for $k \leqslant 10$.

k	2	3	4	5	6	10
η_k/η_1	0.50	0.33	0.25	0.20	0.17	0.11
α_k/α_1	1	1	0.99	0.97	0.94	0.77

In an attempt to generalize this breakage law, we approximate Eq. (2) by an exponential expression,

$$\kappa_{\mathrm{b}}(\sigma) = \alpha_k \exp(\eta_k\sigma), \tag{3}$$

where σ is the stress on the bundle, $\sigma = k\sigma_{\mathrm{f}}$. This form of the breakage rate is exactly equal to Eq. (2) for $k = 1$, where $\alpha_1 = \tau_0^{-1}\exp(-\beta E_{\mathrm{a}})$ and $\eta_1 = \beta\nu$. For $1 < k \leqslant 10$, Eq. (3) approximates Eq. (2) with effective coefficients that are listed in Table I. The k values considered in Table I span the typical range encountered in Nafion-type PEMs [9,10,21]. For $k \gg 1$, Eq. (3) fails to reproduce Eq. (2) in the tail region of large σ. Fits of Eq. (2) by Eq. (3) have been optimized for the range of $\eta_k\sigma$ from 0 to 30 [46].

In the following, we will consider the case with $k = 1$. Under the premise that Eq. (3) remains, to very good approximation, valid for k from 2 to 10, results that we obtain for $k = 1$ can be generalized to k from 2 to 10, using coefficients in Table I.

Upon breakage of a bundle, the load that it carried prior to breaking will be redistributed to surviving bundles in the network. For simplicity, we will assume that the total stress in the network is conserved at each breakage event. We assume that the load redistribution follows a power-law-type redistribution rule, as introduced by Hidalgo *et al.* [18],

$$F(r_{ij}, \gamma) = r_{ij}^{-\gamma}\left(\sum_{j\in I} r_{ij}^{-\gamma}\right)^{-1}, \tag{4}$$

where r_{ij} is the distance between the midpoints of the failed bundle i and an intact bundle j in the lattice, γ is a correlation exponent related to the load distribution range, and I denotes the set of intact bundles. The load transfer function, which describes the load on a surviving bundle j after time step τ, is

$$\sigma_j(t+\tau) = \sigma_j(t+\tau-1) + \sigma_i(t+\tau-1)F(r_{ij}, \gamma), \tag{5}$$

where σ_i is the stress on element i.

The load redistribution rule, adopted in this work for the bundle-network model, is widely used in fiber bundle models (FBMs) of fracture [47,48]. The limit $\gamma \to \infty$ corresponds to the case when the load of the failed bundle is transferred to nearest neighbors, referred to as the local load sharing (LLS) regime. This regime is attained to very good approximation when $\gamma > 10$ [49] The opposite limit, $\gamma \to 0$, corresponds to global load sharing (GLS), wherein all intact bundles receive exactly the same fraction of the load released in the breakage of a bundle. The GLS regime, valid under conditions of low initial stress, represents weakly correlated systems that will be described well as random percolation systems [50]. The case of uncorrelated percolation, studied in Ref. [21], wherein no load redistribution had been considered, is a special case of the GLS regime. Neglecting load redistribution in that approach, as accounted for in the second term on the right-hand side of

Eq. (5), results in an overestimation of the time to fracture. This shortcoming of the previous approach is also being addressed in the present work.

It is important to note that the basic model variant considered in this article assumes that the total stress is conserved. This assumption is usually valid for materials under a controlled external load. However, in the case of a PEM explored here, the stress on bundles is generated internally by water uptake and swelling, and it will usually not be conserved. In future studies using this model, we will introduce a stress dissipation rule to account for the change in total load during crack growth.

III. KINETIC MONTE CARLO SIMULATIONS

A rejection-free kinetic Monte Carlo (MC) method was implemented to simulate the stochastic process of fracture formation on a lattice-type bundle network [29,30,51]. After a time interval τ, one bundle breakage event is randomly selected to happen. The probability that a bundle i is selected is given by

$$p_i = \frac{\kappa_i}{\sum_{j\in I}\kappa_j}, \tag{6}$$

where κ_i is the rate defined in Eq. (3), which depends on the accumulated load σ_i on the bundle. Bundle i is selected if

$$\sum_{j=1}^{i-1} p_j \leqslant \rho^{(1)} < \sum_{j=1}^{i} p_j, \quad i > 1,$$
$$0 \leqslant \rho^{(1)} < p_1, \quad i = 1, \tag{7}$$

where $\rho^{(1)}$ is a random number selected from a uniform distribution [0, 1).

The time interval τ is determined by

$$\tau = -\frac{\ln(\rho^{(2)})}{\sum_{j\in I}\kappa_j}, \tag{8}$$

where $\rho^{(2)}$ is a random number sampled from a uniform distribution [0, 1). Following a breakage event, the load released in the event is redistributed to surviving bundles according to Eqs. (4) and (5). After calculation of the new load distribution, the rates of bundle breakage are recalculated for each intact bundle according to Eq. (3). Moreover, the statistics of clusters of broken bundles is updated at each MC step.

A Monte Carlo run for a given lattice configuration and set of initial parameters is terminated when all bundles are fractured. The percolation threshold is reached when the first cluster of broken bonds is formed that spans across the whole lattice, connecting opposite boundaries in any of the principal directions. The time at which this sample-spanning cluster is formed marks the time to fracture t_{PEM}. We adopt a tree-based algorithm to determine the percolation threshold for finite lattices, following Refs. [52,53].

In this article, we report results for a finite $L \times L$ square lattice with $L = 100$. The number of bundles in the lattice is $N = 2L^2 - 2L$. For each lattice configuration with a given set of values for k, L, γ, σ^0, and T, we perform n independent runs. The percolation thresholds obtained for these n runs (or realizations) exhibit a frequency distribution. For a finite lattice size, the width of this distribution is finite. In the limit of an infinite lattice size, a δ-function-like distribution is approached. From this frequency distribution, an expectation value of the percolation threshold can be determined. In most cases, $n = 5000$–$10\,000$ runs were performed. We employ the ranges of $\eta_k\sigma^0 = 0$–3 and $\gamma = 0$–100 to scan the dynamic range from weakly correlated random breakage to highly locally correlated crack growth.

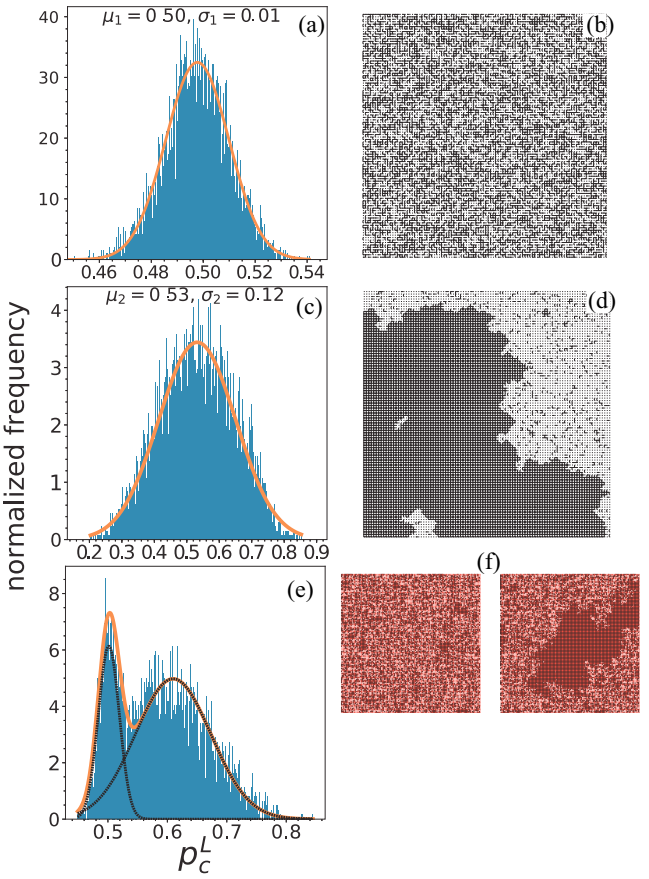

FIG. 2. Normalized frequency distributions of percolation thresholds for a square lattice with $L = 100$, for (a) a random breakage regime ($\eta_k\sigma = 0.20$ and $\gamma = 100$, single Gaussian), (c) a correlated crack growth regime ($\eta_k\sigma = 2.0$ and $\gamma = 100$, single Gaussian), and (e) the crossover region ($\eta_k\sigma^0 = 0.46$ and $\gamma = 10$, two Gaussians). (b), (d), and (f) show snapshots of lattice configurations corresponding to (a), (c), and (e). In the transition region, two clearly distinguishable peaks for random breakage (left) and correlated crack growth (right) are visible and both mechanisms coexist (statistically) on different MC copies, as illustrated in (f).

IV. RESULTS AND DISCUSSION

Figure 2(a) illustrates a frequency distribution of percolation thresholds, obtained with $\eta_k\sigma^0 = 0.20$, $\gamma = 100$, and $n = 5650$. This case falls into the weak correlation regime. The frequency distribution exhibits a single peak and it resembles a Gaussian distribution. In further simulations (not shown), we verified that the width of the distribution decreases with increasing L, approaching a δ-function-like distribution in the $L \to \infty$ limit, as expected.

For networks with strong local correlation, as realized for a large initial stress σ^0 or high γ, the system exhibits correlated crack growth behavior at an early stage. The frequency distribution of percolation thresholds for this case is illustrated in Fig. 2(c), obtained with $\eta_k\sigma^0 = 2.0$, $\gamma = 100$, and $n = 6430$. It exhibits a Gaussian-like shape as well, but with a larger width.

Interestingly, we can identify an intermediate or crossover regime, in which the frequency distribution of percolation thresholds exhibits two peaks, as depicted in Fig. 2(e) for the case $\eta_k\sigma^0 = 0.46$, $\gamma = 10$, and $n = 5000$. In this case, both damage mechanisms, namely, random breakage (left peak) and correlated crack growth (right peak), coexist in a statistical sense. The dominant mechanism of cluster growth for a specific MC realization depends on whether correlated crack growth is triggered at a time point prior to reaching the percolation threshold by uncorrelated cluster growth. Figure 2(f) shows snapshots of MC runs on two different realizations of the system. With the two-peaked shape of the frequency distribution function, we can determine two expectation values of the percolation threshold. The area under the second peak relative to the total area under the distribution function provides a quantitative means to assess the importance of correlation effects for a given lattice configuration and set of conditions.

We reproduce the frequency distributions of percolation thresholds with two Gaussian functions to determine their mean values μ_1, μ_2, standard deviations σ_1, σ_2, and areas A_1, A_2 under the distinct peaks. We define

$$\xi = A_2/(A_1 + A_2) \tag{9}$$

as an order parameter for the transition between random breakage ($\xi \simeq 0$) and correlated crack growth regimes ($\xi \simeq 1$). Moreover, ξ can be employed as a quantitative measure of the strength of local correlations.

Figure 3 depicts how ξ depends on $\eta_k\sigma^0$ and γ. Figure 3(a) shows ξ as a function of σ^0 with γ as parameter, whereas Fig. 3(b) shows ξ as a function of γ with σ^0 as parameter. As can be seen in Fig. 3, for $\eta_k\sigma^0 \leqslant 0.30$ only the first peak ($\xi \sim 0$) occurs over the whole range of γ values explored. In this regime of weak stress, correlated crack growth does not occur. The transition regime, in which two peaks are seen in the frequency distribution plots, extends over narrow ranges of $\eta_k\sigma^0$. For large γ, this range is $0.41 \leqslant \eta_k\sigma^0 \leqslant 0.46$, indicating that the transition from random breakage to correlated crack growth behavior is relatively sharp. Using ξ as an order parameter to explore this transition, we have generated the phase diagram in Fig. 4. The transition region with the statistical coexistence of both damage mechanisms is very narrow, confirming that ξ is a suitable parameter to assess this transition in the plane spanned by $\eta_k\sigma^0$ and γ.

It should be noted that for $\eta_k\sigma^0 > 3.0$, at $\gamma = 1$–2.5, three peaks were observed. At this point, we do not have an explanation for the third peak in terms of another independent damage mechanism.

Figures 5(a) and 5(b) show μ_1 and μ_2 as functions of γ for different values of σ^0. The expectation value of the percolation threshold of the uncorrelated percolation case with $\gamma = 0$ or $\sigma^0 = 0$ is $p_c^{\text{uncor}} = 0.4955 \pm 0.0002$ [54]. As can be seen in Fig. 5(a), μ_1, which represents random breakage

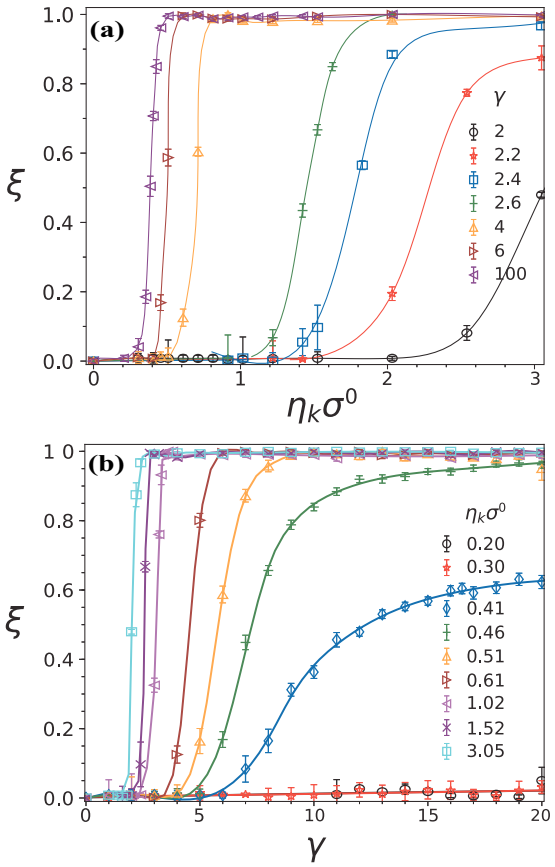

FIG. 3. Plots of the parameter $\xi = A_2/(A_1 + A_2)$ over (a) the initial stress of each bundle σ^0 (scaled by η_k) with γ as the parameter, and (b) γ with σ^0 as the parameter. Interpolated lines are shown to guide the eye.

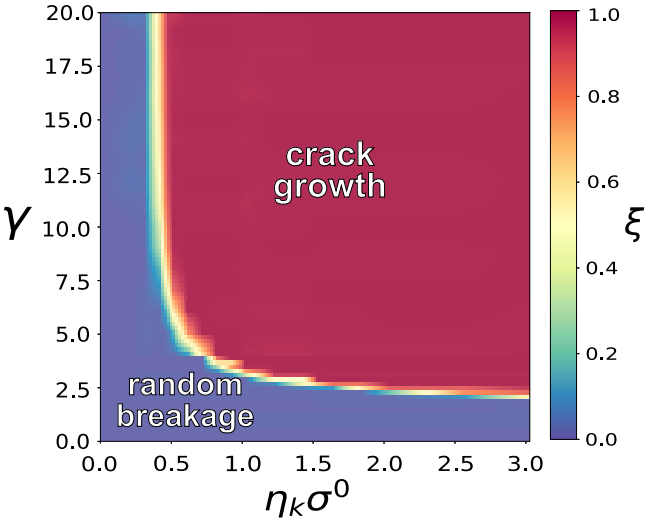

FIG. 4. Phase diagram, illustrated as a color map, in the plane spanned by γ and $\eta_k\sigma^0$. The diagram was generated using Fig. 3 with ξ as the order parameter. Regimes of random breakage and correlated crack growth are clearly discernible, separated by a narrow crossover region.

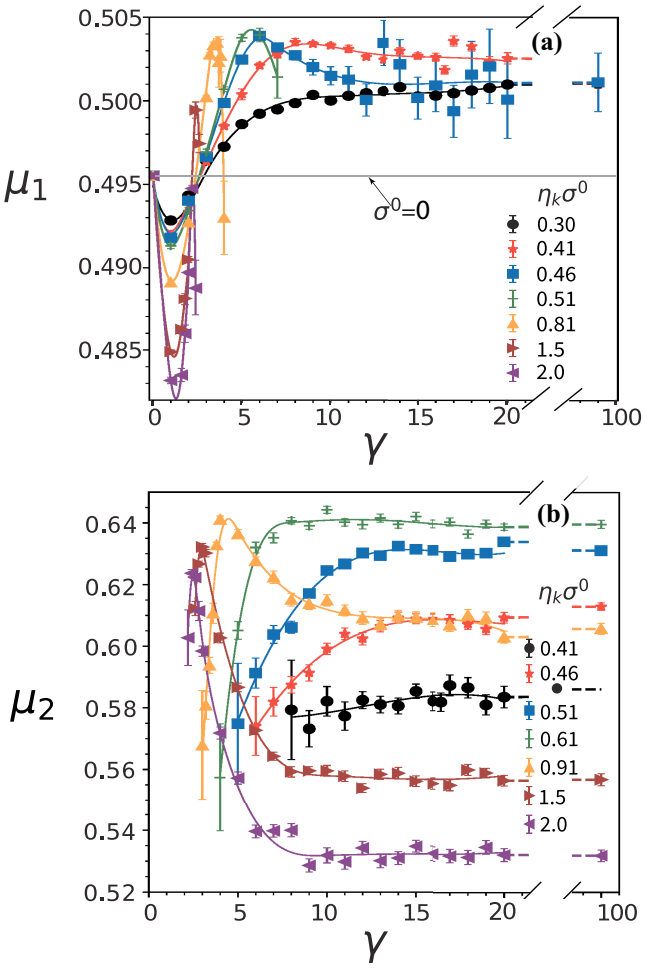

FIG. 5. Plots of (a) μ_1 and (b) μ_2 as a function of γ with $\eta_k\sigma^0$ as the parameter.

events, closely approaches this value. As a function of γ, μ_1 decreases at first. At $\xi \sim 0$, corresponding to a long-range correlated system, an increase in the strength of local correlations helps the growth on several clusters, accelerating cluster merging and thereby promoting the formation of the spanning cluster. Similar behavior was observed for long-range correlated systems explored in Refs. [55–61]. The minimum in μ_1 is found at around $\gamma = 1$–2. As the local correlation becomes even stronger upon a further increase of γ, growth happens at one or a few clusters only, which is not contributing to connecting clusters. The variation of μ_1 is, however, small.

More significant changes are seen in the plot of μ_2 as a function of γ. The values of μ_2 vary in the range $0.53 \leqslant \mu_2 \leqslant 0.64$. In the regime of weak initial stress, μ_2 increases from an initially low value at small γ to asymptotically approach a plateau value for $\gamma \geqslant 10$. At a high initial stress, $\eta_k\sigma^0 > 0.5$, μ_2 goes through a sharp maximum at small γ and then relaxes to a lower plateau upon increasing γ. The larger is $\eta_k\sigma^0$, the sharper is the maximum and the lower is the plateau value. As for μ_2 as a function of $\eta_k\sigma^0$ (not shown), it first rises and then drops for all γ. The drop in the percolation threshold with the increase of the correlation strength was previously reported in Ref. [62].

For $\eta_k\sigma^0 < 3.0$, the variances of both peaks in the distribution of percolation thresholds, viz., σ_1 and σ_2, increase with ξ, but the peak due to random breakage is narrower, with σ_1 in the range 0.01–0.02, whereas σ_2 lies in the range 0.05–0.12. In the correlated crack growth regime, the fracture formation on the lattice is dominated very strongly by the largest crack, which exhibit a large variability in shape, among different simulation runs, resulting in the larger σ_2. In the random breakage regime, percolation clusters exhibit a high degree of similarity for different simulation runs performed at a given set of parameters, resulting in a narrow peak in the probability distribution of percolation thresholds. The general trends are that σ_1 and σ_2 increase with increasing $\eta_k\sigma^0$ and γ, with the more regular and pronounced trends seen in σ_2. High sensitivities of σ_2 to these parameters are seen in the random breakage regime. In the correlated crack growth regime, at $\gamma > 5$, σ_2 becomes independent of γ. The variations of σ_1 and σ_2 with L will be analyzed in our forthcoming study.

To gain further insight into percolation behavior and the underlying damage growth mechanisms, we analyze the size of the largest cluster of broken bonds S_L (normalized to N) as a function of the fraction of failed bonds in Fig. 6. For damage propagation by random breakage, the formation of the sample-spanning cluster proceeds in three stages, illustrated with the red solid line in Fig. 6(a): (I) random nucleation of isolated cracks (slope ~ 0); (II) merging of cracks into larger clusters (slope $\gg 1$); and (III) growth of the largest crack (slope ~ 1). Regardless of the overall correlation strength, viz., γ, stage I is always observed since the initial stress is uniformly distributed on the lattice. As $\eta_k\sigma^0$ or γ become larger, i.e., the system shifts towards the crack growth regime in Fig. 4, the merging stage is becoming less pronounced. In this regime, correlated growth of a single crack dominates. Eventually, for systems with $\xi \sim 1$ (dashed-dotted line), a direct transition from stage I to stage III occurs, bypassing the merging stage II. Upon increasing the value of ξ, the accumulation of stress on the largest crack is accelerating, which has a significant impact on the correlated crack growth regime, affecting the percolation threshold and time to fracture. This strong acceleration effect is due to the exponential breakage rule. The effect is much weaker if a power-law breakage rule is considered, as in Ref. [19], in contrast to the unchanged fracture pattern in the study of Ref. [63] even for the LLS scheme.

Figure 6 illustrates the growth of the largest cluster in three stress ranges: $\eta_k\sigma^0 = 0.30$ [Fig. 6(b)], $\eta_k\sigma^0 = 0.46$ [Fig. 6(c)], and $\eta_k\sigma^0 = 2.0$ [Fig. 6(d)]. S_L varies from GLS to LLS, corresponding to different damage mechanisms. When $\eta_k\sigma^0 = 0.30$, the overlap of the S_L curves in Fig. 6(b) indicates that only the random breakage mechanism occurs, consistent with $\xi \sim 0$ for $\sigma^0 \leqslant 0.30$ in Fig. 3. As for Fig. 6(c), representing the crossover region, as shown by the shaded area, correlated crack growth was not observed even for the extreme case of LLS (i.e., for large γ). But the merging stage is shrinking, indicating the transition to correlated crack growth. In Fig. 6(d), all three pathways of formation and growth of clusters are present, corresponding to the parameter ranges $0 \leqslant \xi \leqslant 2$ (random breakage regime), $2.2 \leqslant \xi \leqslant 2.4$ (crossover region), and $\xi \geqslant 2.6$ (correlated crack growth regime).

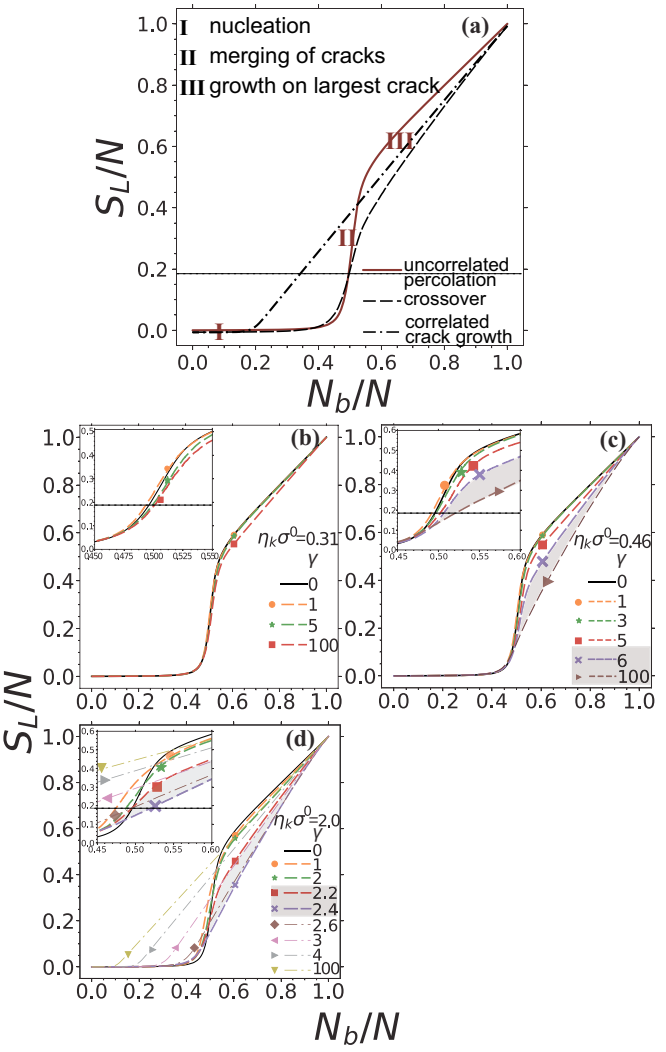

FIG. 6. Normalized growth of the maximum crack size S_L/N with the fraction of failed bonds in the lattice. The horizontal dashed lines in (a) and in the insets of (b)–(d) indicate the size of the largest cluster in the uncorrelated percolation case. In (a), three regimes are shown—random breakage (red solid line), crossover, where $0 < \xi < 1$ (dashed line), and correlated crack growth (dashed-dotted line)—and three growth stages are indicated: (I) nucleation of cracks, (II) merging of cracks, and (III) growth concentrated on the largest crack. Cluster growth is shown for different range regimes in (b) with $\eta_k\sigma^0 = 0.30$, (c) with $\eta_k\sigma^0 = 0.46$, and (d) with $\eta_k\sigma^0 = 2.0$. The shaded area indicates the crossover region where $0 < \xi < 1$.

Next, we analyze the time to fracture t_{PEM} for the evaluated ranges of σ^0 and γ. Results are displayed in Fig. 7. The frequency distribution of t_{PEM} values, obtained in each case over n MC runs performed under identical conditions, is shown for three different systems, with details given in the caption. It exhibits a single peak for the random breakage regime, i.e., for $\xi \sim 0$, shown in Fig. 7(a), as well as in the correlated crack growth regime with $\xi \sim 1$, shown in Fig. 7(c). A combination of two peaks can be discerned in the crossover regime, Fig. 7(b). Using these distributions, we have calculated the expectation value of t_{PEM}, which is depicted as a function of $\eta_k\sigma^0$ with γ as the parameter in Fig. 8(a), and, alternatively, as a function of γ with $\eta_k\sigma^0$ as the parameter

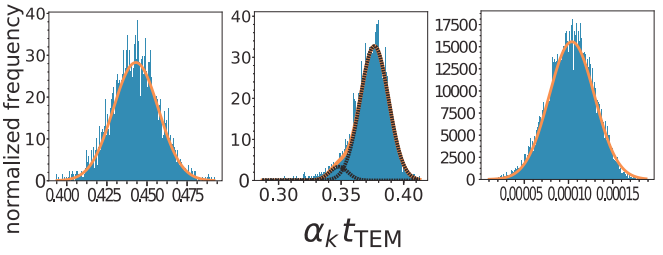

FIG. 7. Frequency distributions of the time to fracture t_{PEM} (normalized to α_k) for systems in the regime of random breakage (left, $\eta_k\sigma^0 = 0.30$ and $\gamma = 4.0$), crossover (middle, $\eta_k\sigma^0 = 0.41$, $\gamma = 10$), and correlated crack growth (right, $\eta_k\sigma^0 = 5.0$, $\gamma = 100$). The distribution in the crossover region exhibits a superposition of two Gaussian peaks.

in Fig. 8(b). Due to the exponential bundle breakage law, introduced in Eq. (2), t_{PEM} follows essentially an exponential dependence on $\eta_k\sigma^0$.

Figure 8(b) displays t_{PEM} as a function of γ. It exhibits a peculiar transition between two plateaus, from a higher value in the random breakage regime (or GLS regime), attained for $\gamma < 2$, to a lower value in the correlated crack growth regime (LLS regime) that is approached asymptotically for $\gamma > 5$.

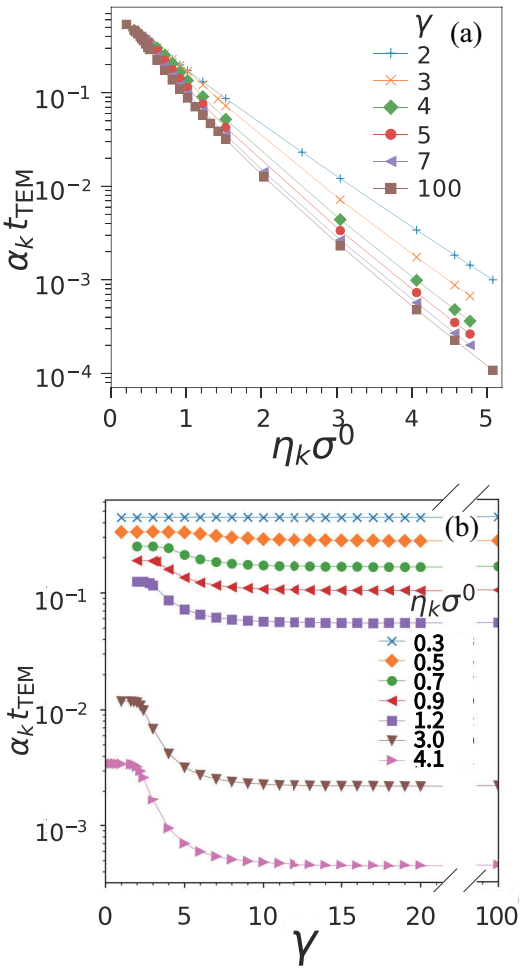

FIG. 8. Time to fracture (normalized to α_k) (a) on a log scale as a function of $\eta_k\sigma^0$ with γ as the parameter and (b) as a function of γ with $\eta_k\sigma^0$ as the parameter.

TABLE II. Lifetime for $k = 1, 3, 10$ at $T = 298$ and 353 K in the range of $\sigma^0 = 3$–30 MPa. The two limits for the range of t_{PEM} values given in parentheses correspond to γ varying from 0 to 100, respectively.

k	σ^0 (MPa)	$T = 298$ K, t_{PEM} (h)	$T = 353$ K, t_{PEM} (h)
1	3	4.2×10^5[a]	2.5×10^2[a]
	5	$(3.1–2.6) \times 10^5$	$(2.0–1.6) \times 10^2$
	30	$(11–2.1) \times 10^3$	6.9–1.3
3	3	5×10^5[b]	3×10^2[b]
	5	5×10^5[b]	3×10^2[b]
	30	$(16–8) \times 10^4$	$(10–5.0) \times 10^1$
10	3	6×10^5[b]	4×10^2[b]
	5	6×10^5[b]	4×10^2[b]
	30	3.2×10^5[a]	2.0×10^2[a]

[a]The changes of these values of t_{PEM} are insignificant when varying γ.

[b]These values corresponds to $\eta_k \sigma^0 < 0.2$, in which the data were not obtained. We approximated the values by extrapolating data in Fig. 8(a).

The magnitude of the transition shows a high sensitivity to $\eta_k \sigma^0$. At the highest stress value included in the plot, the two plateaus differ by a factor of 10, whereas at low stress values the transition becomes insignificant. These observations illustrate the concerted impact of stress and the effective range of stress transfer on the dynamics of the percolation transition. The position of the transition region on the γ axis is rather insensitive to $\eta_k \sigma^0$. We notice similar observations in the dynamic fracture behaviors reported in Refs. [18,64], with a crossover from global to local load sharing occurring at a critical value γ_c that is found around $\gamma = 2$, in agreement with our findings. In the latter studies the property monitored is the ultimate or critical stress, defined as the maximum load the material can sustain before it breaks down.

Table II shows the dimensional lifetime t_{TEM} (hours) obtained with our model for $\sigma^0 = 3$, 5, and 30 MPa, bundle sizes $k = 1, 3, 10$, and $T = 298$ and 353 K. We use $\tau_0 = 1.0 \times 10^{-11}$ s, $E_a = 1.95 \times 10^{-22}$ kJ, $\nu = 0.418$ nm^3 [45], as well as the parameters in Table I for the calculations of α_k and η_k. As can be seen, temperature has a marked impact on t_{TEM}, with the higher T destabilizing the bundle network. Moreover, t_{TEM} decreases with increasing σ^0, whereas a larger k has a stabilizing effect. While all these trends are reasonable, it will be important in future work to evaluate t_{TEM} for more realistic lattice configurations in 3D.

V. CONCLUSIONS

In this article, a random network model was developed to predict the lifetime of polymer electrolyte membranes (PEMs). The model also provides general physical insights into the problem of correlated bond percolation on a fracture network under an exponential breakdown rule for bonds in the network and a power-law stress transfer rule (r^γ). Correlation in the fracture system is described by the exponent γ, which controls the effective range of stress transfer and the initial stress σ^0, which was assumed to be uniformly distributed in this work. Results highlight the crossover between the two limiting regimes: percolationlike random breakage in the limit of weak correlation and crack growth in the limit of strong local correlation. The following main conclusions can be drawn:

(1) In the crossover region, the frequency distribution of percolation threshold exhibits two Gaussian-like peaks. The area of the second peak can be employed as an order parameter to assess the strength of local correlations. Accordingly, we generated the phase diagram of two limiting regimes and their crossover in the plane spanned by σ^0 and γ.

(2) Although the percolation thresholds may be intuitively expected to drop with the increase of the correlation strength, we observe this slight drop only when the local correlation is very weak. Under stronger correlation, however, the percolation thresholds grow even higher than that of the uncorrelated case and eventually drop again when transiting to the regime of correlated crack growth.

(3) We analyzed the growth dynamics on the largest cluster in the different regimes. For correlated crack growth, the merging phase is skipped.

(4) The statistics of percolation clusters was used for a lifetime assessment of PEMs. The lifetime decreases exponentially with σ^0. For a larger initial stress σ^0, the local load sharing (LLS) regime significantly reduces the lifetime of PEMs. As a function of γ, the PEM lifetime exhibits a transition from a higher plateau at $\gamma < 2$ to a lower plateau at $\gamma > 10$.

A possible extension of this work will be to construct a phase diagram with the size of the lattice as an additional degree of freedom. The current analysis is limited to lattices with $L = 100$. It will be interesting to assess within the present approach how fracture propagates when approaching the limit of infinite lattice size. Preliminary studies for a limited range of σ^0 and γ values have revealed a transition from random breakage to correlated crack growth with increasing lattice size. According to Shekhawat *et al.* [1] in their work on fuse networks, the random breakage regime is just a finite-size effect. Moreover, we have seen in preliminary calculations (not shown here) that the time-to-fracture of the network decreases with system size. Similar observations had been made in the works of FBM models by Melchy and Eikerling [21] and Yewande *et al.* [19]. This counterintuitive observation is due to the assumption that the total stress is conserved. As a result, a larger total amount of stress is present in larger systems. Introducing a stress dissipation rule will result in qualitatively different fracture propagation behavior for $L \to \infty$.

For the practical goal of making realistic predictions about the lifetime of PEMs, in future work we will study three-dimensional bundle networks with nonuniform distributions of bundle sizes, stiffness, elastic modulus, and surface charge density, as well as inhomogeneous initial stress distributions.

ACKNOWLEDGMENTS

We thank M. Kennett (Simon Fraser University) and N. Lee-Hone (Simon Fraser University) for fruitful discussions. The work was supported by the Natural Sciences and Engineering Research Council of Canada through the Discovery Grants program (RGPIN-2014-04074).

[1] A. Shekhawat, S. Zapperi, and J. P. Sethna, Phys. Rev. Lett. **110**, 185505 (2013).
[2] F. T. Pierce, J. Text. Inst. **17**, T355 (1926).
[3] R. Albert and A.-L. Barabási, Rev. Mod. Phys. **74**, 47 (2002).
[4] M. Eikerling and A. Kulikovsky, *Polymer Electrolyte Fuel Cells: Physical Principles of Materials and Operation* (CRC Press, Boca Raton, FL, 2014).
[5] A. Kraytsberg and Y. Ein-Eli, Energy Fuels **28**, 7303 (2014).
[6] X. Huang, R. Solasi, Y. Zou, M. Feshler, K. Reifsnider, D. Condit, S. Burlatsky, and T. Madden, J. Polym. Sci., Part B: Polym. Phys. **44**, 2346 (2006).
[7] H. Wang, H. Li, and X.-Z. Yuan, *PEM Fuel Cell Failure Mode Analysis*, Vol. 1 (CRC Press, Boca Raton, FL, 2011).
[8] E. Kjeang, N. Djilali, and D. Sinton, J. Power Sources **186**, 353 (2009).
[9] P.-É. A. Melchy and M. H. Eikerling, Phys. Rev. E **89**, 032603 (2014).
[10] M. Ghelichi, K. Malek, and M. H. Eikerling, Macromolecules **49**, 1479 (2016).
[11] R. Hiesgen, S. Helmly, I. Galm, T. Morawietz, M. Handl, and K. Friedrich, Membranes **2**, 783 (2012).
[12] A. S. Ioselevich, A. A. Kornyshev, and J. H. G. Steinke, J. Phys. Chem. B **108**, 11953 (2004).
[13] L. Rubatat, A. L. Rollet, G. Gebel, and O. Diat, Macromolecules **35**, 4050 (2002).
[14] L. Rubatat, G. Gebel, and O. Diat, Macromolecules **37**, 7772 (2004).
[15] M. H. Eikerling and P. Berg, Soft Matter **7**, 5976 (2011).
[16] M. Safiollah, P.-E. A. Melchy, P. Berg, and M. Eikerling, J. Phys. Chem. B **119**, 8165 (2015).
[17] P. Hamilton and B. Pollet, Fuel Cells **10**, 489 (2010).
[18] R. C. Hidalgo, Y. Moreno, F. Kun, and H. J. Herrmann, Phys. Rev. E **65**, 046148 (2002).
[19] O. E. Yewande, Y. Moreno, F. Kun, R. C. Hidalgo, and H. J. Herrmann, Phys. Rev. E **68**, 026116 (2003).
[20] S. Zapperi, P. K. V. V. Nukala, and S. Šimunović, Phys. Rev. E **71**, 026106 (2005).
[21] P.-É. A. Melchy and M. H. Eikerling, J. Phys.: Condens. Matter **27**, 325103 (2015).
[22] D. Sornette, J. Phys. I (France) **2**, 2089 (1992).
[23] P. C. Hemmer and A. Hansen, J. Appl. Mech. **59**, 909 (1992).
[24] D. L. Turcotte, *Fractals and Chaos in Geology and Geophysics* (Cambridge University Press, Cambridge, UK, 1997).
[25] S. Biswas, S. Roy, and P. Ray, Phys. Rev. E **91**, 050105(R) (2015).
[26] D. T. Gillespie, J. Comput. Phys. **22**, 403 (1976).
[27] D. Ceperley and M. Kalos, in *Monte Carlo Methods in Statistical Physics*, edited by K. Binder (Springer, Heidelberg, 1979).
[28] A. Jansen, Comput. Phys. Commun. **86**, 1 (1995).
[29] S. A. Serebrinsky, Phys. Rev. E **83**, 037701 (2011).
[30] M. J. Hoffmann, S. Matera, and K. Reuter, Comput. Phys. Commun. **185**, 2138 (2014).
[31] W. A. Curtin and H. Scher, Phys. Rev. Lett. **67**, 2457 (1991).
[32] D. Y. Galperin and A. R. Khokhlov, Macromol. Theory Simul. **15**, 137 (2006).
[33] J. T. Wescott, Y. Qi, L. Subramanian, and T. Weston Capehart, J. Chem. Phys. **124**, 134702 (2006).
[34] N. Grønbech-Jensen, R. J. Mashl, R. F. Bruinsma, and W. M. Gelbart, Phys. Rev. Lett. **78**, 2477 (1997).
[35] J. Barrat and J. Joanny, Adv. Chem. Phys. **94**, 1 (1996).
[36] B.-Y. Ha and A. J. Liu, Phys. Rev. Lett. **79**, 1289 (1997).
[37] M. J. Stevens, Phys. Rev. Lett. **82**, 101 (1999).
[38] L. Guldbrand, L. G. Nilsson, and L. Nordenskiöld, J. Chem. Phys. **85**, 6686 (1986).
[39] T. Mima, T. Kinjo, S. Yamakawa, and R. Asahi, Soft Matter **13**, 5991 (2017).
[40] M. Eikerling, A. Kornyshev, A. Kuznetsov, J. Ulstrup, and S. Walbran, J. Phys. Chem. B **105**, 3646 (2001).
[41] G. Gebel, Polymer **41**, 5829 (2000).
[42] D. Stauffer and A. Aharony, *Introduction to Percolation Theory* (Taylor & Francis, London, 2018).
[43] M. J. Alava, P. Nukala, and S. Zapperi, Adv. Phys. **55**, 349 (2006).
[44] C. Lim, L. Ghassemzadeh, F. Van Hove, M. Lauritzen, J. Kolodziej, G. Wang, S. Holdcroft, and E. Kjeang, J. Power Sources **257**, 102 (2014).
[45] S. Zhurkov and V. Korsukov, J. Polym. Sci., Polym. Phys. Ed. **12**, 385 (1974).
[46] The upper limit of the evaluated range of $\eta_k\sigma$ is approximately determined by the highest stress on a single bundle when 50% bundles have failed for the system of $\eta\sigma^0 = 0.46$ and $\gamma = 100$.
[47] S. Pradhan, A. Hansen, and B. K. Chakrabarti, Rev. Mod. Phys. **82**, 499 (2010).
[48] J. Lehmann and J. Bernasconi, Chem. Phys. **375**, 591 (2010).
[49] For $\gamma > 10$, nearest neighbors share 96.8% of the load released by a broken bundle. In our study, the highest γ is set to be 100, for which 99.999 97% are shared with nearest neighbors.
[50] It is to be noted that the strength of correlations depends on both parameters γ and σ^0. In studies of Ref. [18] by Hidalgo *et al.*, breakage events in the network were assumed to follow a power-law breakdown rule and the fracture process was independent of the uniformly distributed initial stress. In our case, however, the breakage rate of bundles follows an exponential law. The probability of a bundle to fail at each kinetic MC step is proportional to its rate. In the power-law case, the ratio of breakage possibilities between a bundle with $n\sigma^0$ and another bundle with σ^0 does not change, i.e., $\frac{d}{d\sigma^0}\frac{n\sigma^{0\rho}}{\sigma^{0\rho}} = 0$. In our case, bundles with larger stress are more strongly correlated in systems with larger initial stress, and thus $\frac{d}{d\sigma^0}\frac{\exp(n\eta_k\sigma^0)}{\exp(\eta_k\sigma^0)} > 0$ for $n > 1$.
[51] K. Binder, D. Heermann, L. Roelofs, A. J. Mallinckrodt, and S. McKay, Comput. Phys. **7**, 156 (1993).
[52] M. E. J. Newman and R. M. Ziff, Phys. Rev. Lett. **85**, 4104 (2000).
[53] M. E. J. Newman and R. M. Ziff, Phys. Rev. E **64**, 016706 (2001).
[54] For an infinite square lattice, the exact percolation threshold is $p_c = 0.5$ [42] .
[55] A. Weinrib, Phys. Rev. B **29**, 387 (1984).
[56] K. J. Schrenk, N. Posé, J. J. Kranz, L. V. M. Van Kessenich, N. A. M. Araújo, and H. J. Herrmann, Phys. Rev. E **88**, 052102 (2013).
[57] S. Prakash, S. Havlin, M. Schwartz, and H. E. Stanley, Phys. Rev. A **46**, R1724(R) (1992).

[58] N. Araújo, P. Grassberger, B. Kahng, K. J. Schrenk, and R. M. Ziff, Eur. Phys. J.: Spec. Top. **223**, 2307 (2014).
[59] K. S. Mendelson, Phys. Rev. E **56**, 6586 (1997).
[60] T. Harter, Phys. Rev. E **72**, 026120 (2005).
[61] P. Renault, Transp. Porous Media **6**, 451 (1991).
[62] M. R. Riedel and S.-i. Karato, Geophys. J. Int. **125**, 397 (1996).
[63] Z. Danku and F. Kun, J. Stat. Mech.: Theory Exp. **2016**, 73211.
[64] F. Raischel, F. Kun, and H. J. Herrmann, Phys. Rev. E **74**, 035104(R) (2006).

Correction: Minor errors in Table II have been fixed.